

Activation of Store-Operated Calcium Entry in Airway Smooth Muscle Cells: Insight from a Mathematical Model

Huguette Croisier^{1*}, Xiahui Tan², Jose F. Perez-Zoghbi³, Michael J. Sanderson², James Sneyd⁴, Bindi S. Brook¹

1 School of Mathematical Sciences, University of Nottingham, Nottingham, United Kingdom, **2** Department of Microbiology and Physiological Systems, University of Massachusetts Medical School, Worcester, Massachusetts, United States of America, **3** Department of Cell Physiology and Molecular Biophysics, Texas Tech University Health Sciences Center, Lubbock, Texas, United States of America, **4** Department of Mathematics, University of Auckland, Auckland, New Zealand

Abstract

Intracellular Ca^{2+} dynamics of airway smooth muscle cells (ASMC) mediate ASMC contraction and proliferation, and thus play a key role in airway hyper-responsiveness (AHR) and remodelling in asthma. We evaluate the importance of store-operated Ca^{2+} entry (SOCE) in these Ca^{2+} dynamics by constructing a mathematical model of ASMC Ca^{2+} signaling based on experimental data from lung slices. The model confirms that SOCE is elicited upon sufficient Ca^{2+} depletion of the sarcoplasmic reticulum (SR), while receptor-operated Ca^{2+} entry (ROCE) is inhibited in such conditions. It also shows that SOCE can sustain agonist-induced Ca^{2+} oscillations in the absence of other Ca^{2+} influx. SOCE up-regulation may thus contribute to AHR by increasing the Ca^{2+} oscillation frequency that in turn regulates ASMC contraction. The model also provides an explanation for the failure of the SERCA pump blocker CPA to clamp the cytosolic $[\text{Ca}^{2+}]_i$ of ASMC in lung slices, by showing that CPA is unable to maintain the SR empty of Ca^{2+} . This prediction is confirmed by experimental data from mouse lung slices, and strongly suggests that CPA only partially inhibits SERCA in ASMC.

Citation: Croisier H, Tan X, Perez-Zoghbi JF, Sanderson MJ, Sneyd J, et al. (2013) Activation of Store-Operated Calcium Entry in Airway Smooth Muscle Cells: Insight from a Mathematical Model. PLoS ONE 8(7): e69598. doi:10.1371/journal.pone.0069598

Editor: Laszlo Csernoch, University of Debrecen, Hungary

Received: February 14, 2013; **Accepted:** June 10, 2013; **Published:** July 25, 2013

Copyright: © 2013 Croisier et al. This is an open-access article distributed under the terms of the Creative Commons Attribution License, which permits unrestricted use, distribution, and reproduction in any medium, provided the original author and source are credited.

Funding: BSB acknowledges funding from the Medical Research Council (<http://www.mrc.ac.uk>), New Investigator Grant: G0901174. MJS is supported by a grant from National Institutes of Health (<http://www.nih.gov>): HL103405. The funders had no role in study design, data collection and analysis, decision to publish, or preparation of the manuscript.

Competing Interests: The authors have declared that no competing interests exist.

* E-mail: Huguette.Croisier@nottingham.ac.uk

Introduction

Ca^{2+} is a ubiquitous cellular messenger, controlling a wide range of biological functions. These include ASMC contraction and proliferation, which are associated with airway hyper-responsiveness (enhanced contractility) and airway remodelling (structural changes) in asthma. The main trigger for cytoplasmic Ca^{2+} ($[\text{Ca}^{2+}]_i$) increase in ASMC is agonist stimulation at the cell membrane (e.g., by histamine released from mast cells or acetylcholine released from nerves). Binding of agonist to G-protein coupled receptors induces the production of IP_3 , a second messenger which diffuses into the cytosol and binds to IP_3 receptor Ca^{2+} channels (IPR) on the sarcoplasmic reticulum (SR) membrane (Fig. 1). This causes the IPR to open and release Ca^{2+} from the SR into the cytosol (the SR being the main Ca^{2+} store in ASMC). As $[\text{Ca}^{2+}]_i$ exerts a positive feedback on IPR, this results in so-called Ca^{2+} -induced Ca^{2+} release (CICR). The release is terminated by the inhibition of the IPR at large $[\text{Ca}^{2+}]_i$, and Ca^{2+} is pumped back into the SR by Ca^{2+} ATP-ases (SERCA). Hence, for sufficient IP_3 concentration, cycling of Ca^{2+} through IPR can occur, and give rise to the repetitive propagation of $[\text{Ca}^{2+}]_i$ waves through the cytosol. These appear as $[\text{Ca}^{2+}]_i$ oscillations at the whole-cell level. Importantly, airway contraction increases with the frequency of these $[\text{Ca}^{2+}]_i$ oscillations [1,2]. Ca^{2+} dynamics are also involved in ASMC proliferation [3–5],

and in the assembly of myosin thick filament and actin thin filament [6–8], which form the contractile machinery of ASMC. In addition, several Ca^{2+} channels and pumps in ASMC are regulated by inflammatory mediators present in asthma (e.g., [4,9–12]). Ca^{2+} dynamics therefore appear to be involved in multiple interrelated aspects of asthma at the cellular level. In the present work, we use mathematical modelling to investigate the important Ca^{2+} pathways at play in Ca^{2+} dynamics of ASMC and thus improve our understanding of airway hyper-responsiveness and remodelling in asthma.

Store-operated Ca^{2+} entry (SOCE) is one important Ca^{2+} entry mechanism, in which plasma membrane (PM) Ca^{2+} channels open in response to Ca^{2+} store depletion. These are called store-operated Ca^{2+} channels (SOCC). Although the concept of SOCE was proposed 25 years ago [13], the mechanism of its activation has been identified only recently [14]. The process is mediated by stromal interaction molecules (STIM), proteins embedded in the SR membrane which are sensitive to SR Ca^{2+} . Upon dissociation of Ca^{2+} from their SR binding site, they oligomerise and translocate within the SR membrane to the plasma membrane. Here, STIM proteins bind to Orai and/or TRP, the proteins forming the pore of SOCC, and trigger their opening (Fig. 1). Although SOCE has been identified in many cells, it is generally stimulated by artificial emptying of the Ca^{2+} store, as there is unfortunately no specific pharmacological SOCC

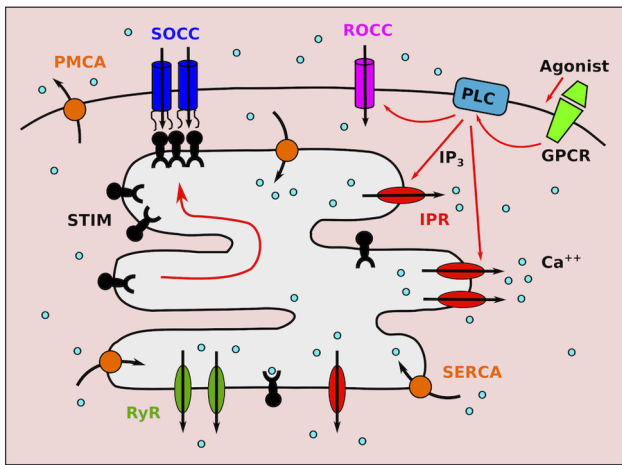


Figure 1. Schematic of Ca^{2+} signalling in ASM cell. Agonist stimulation of G-protein coupled receptors (GPCR) induces PLC β activation, giving rise to IP $_3$ production and Ca^{2+} entry through receptor-operated Ca^{2+} channels (ROCC). IP $_3$ triggers Ca^{2+} release through IPR. Depletion of the SR from Ca^{2+} causes STIM protein oligomerisation and migration toward the cell membrane, where they bind and activate store-operated Ca^{2+} channels (SOCC). Ca^{2+} ATPases pump Ca^{2+} back into the SR (SERCA) and out of the cell (PMCA). doi:10.1371/journal.pone.0069598.g001

blocker. Hence, the importance of store depletion, and therefore of SOCE, during physiological conditions such as Ca^{2+} oscillations, remains largely unknown. This may explain why SOCE has been included only in a few mathematical models of Ca^{2+} dynamics [15–18]. In particular, no prior modelling work on Ca^{2+} dynamics in ASM cell [19–23] has taken SOCE into account, even though there is evidence that SOCE is up-regulated by inflammatory mediators found in asthma (TNF- α and IL-13) [9,11,24], and is associated with ASM cell proliferation [3,5].

In this paper, we develop a mathematical model to evaluate the importance of SOCE in Ca^{2+} dynamics of ASM cell. While there is much evidence that SOCE occurs upon SR depletion in cultured ASM cell *in vitro* (e.g., [3,25–27]), these cultured cells often lose their contractile phenotype, and rarely display agonist-induced Ca^{2+} oscillations. Hence, ASM cell in lung slices, which retain most of their physiological and morphological characteristics, are a more reliable preparation to study ASM cell $[\text{Ca}^{2+}]_i$ dynamics. Moreover, the available data from lung slices reflect $[\text{Ca}^{2+}]_i$ dynamics in individual ASM cell, while the majority of works with cultured cells provide only global imaging of $[\text{Ca}^{2+}]_i$ over wells containing thousands of ASM cell. Therefore, we base our model on data from lung slices. SOCE has not been studied directly in lung slices, but a treatment with ryanodine-cafeine (Rya-Caf) has previously been used to clamp the cytosolic Ca^{2+} of ASM cell [2,28,29], which relies on emptying the SR from Ca^{2+} . The results of these experiments therefore provide invaluable information about SOCE. Because agonist stimulation was systematically performed before Rya-Caf treatment to ensure that the lung slice is viable, i.e., that ASM cell exhibit normal $[\text{Ca}^{2+}]_i$ oscillations and contraction, we can construct a mathematical model of $[\text{Ca}^{2+}]_i$ dynamics informed by these data that accounts for both physiological and non-physiological conditions. The model is then used to i) evaluate the effect of SOCE up- and down-regulation on agonist-induced $[\text{Ca}^{2+}]_i$ oscillations, and ii) explain the inability of the SERCA pump blocker CPA to clamp the $[\text{Ca}^{2+}]_i$, in contrast with Rya-Caf treatment.

Methods

Ethics Statement

The experimental study followed the recommendations in the Guide for the Care and Use of Laboratory Animals of the National Institutes of Health. The protocol was approved by the Institutional Animal Care Committee of the University of Massachusetts Medical School (Docket Number: A-836-12). Animals were euthanized with sodium pentobarbital before tissue collection.

Experimental data

Data consist of fluorescence recordings of $[\text{Ca}^{2+}]_i$ dynamics in ASM cell within intact lung slices. All the materials and methods have been previously described (e.g., [2,28]). Essentially, $[\text{Ca}^{2+}]_i$ imaging was performed from regions of about $4\mu\text{m}^2$ within ASM cell (Fig. 2), using two-photon laser scanning microscopy. The fluorescent indicator employed was Oregon Green BAPTA-1-AM, which has a high affinity for Ca^{2+} ($K_d \approx 0.2\mu\text{M}$). We use published data [2] to develop the mathematical model, and new experimental results to test the model predictions (see Results). The latter data can be made freely available upon request for academic, non-commercial use.

Mathematical model

Intracellular Ca^{2+} dynamics are modelled at the whole-cell level, via the following system of ordinary differential equations (e.g., [30]):

$$\begin{aligned} \frac{dc}{dt} &= J_{in} - J_{PMCA} + J_{rel} - J_{SERCA}, \\ \frac{dc_s}{dt} &= \gamma(J_{SERCA} - J_{rel}), \end{aligned} \quad (1)$$

where $c = [\text{Ca}^{2+}]_i$ is the free cytosolic Ca^{2+} concentration, and $c_s = [\text{Ca}^{2+}]_{SR}$ is the free SR Ca^{2+} concentration.

The term J_{in} represents the total influx of Ca^{2+} into the cytosol through PM channels; J_{PMCA} , the Ca^{2+} efflux through the PM Ca^{2+} ATP-ase pumps (PMCA); J_{rel} , the Ca^{2+} flux of Ca^{2+} from the SR into the cytosol, and J_{SERCA} , the flux of Ca^{2+} from the cytosol into the SR through the SR/ER Ca^{2+} ATP-ases

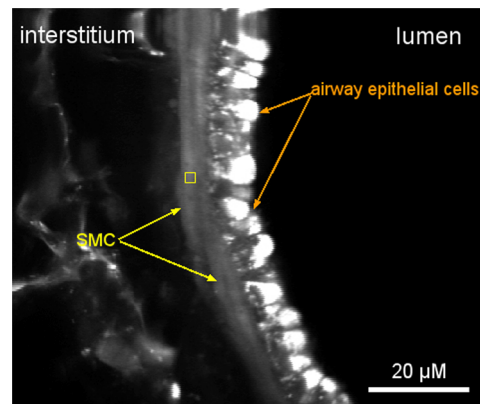


Figure 2. Fluorescence image of part of a mouse airway wall obtained by two-photon laser scanning microscopy. The yellow square shows a typical region, within an ASM cell, from which Ca^{2+} dynamics is imaged. doi:10.1371/journal.pone.0069598.g002

(SERCA). The factor γ represents the ratio of cytoplasmic volume to SR volume, and implicitly incorporates the relative effect of fast, linear (e.g., low affinity) Ca²⁺ buffers in the SR compared to the effect of similar buffers in the cytosol. Indeed, the effect of fast, linear buffers amounts to a global rescaling of the Ca²⁺ fluxes in the corresponding compartment (e.g., [30]). The other buffers are assumed to have a negligible effect on Ca²⁺ dynamics at the whole-cell level (see also Discussion).

We assume that

$$J_{in} = J_{leakin} + J_{ROCC} + J_{SOCC}, \quad (2)$$

where J_{leakin} is a constant Ca²⁺ leak through unspecified channels, J_{ROCC} is the Ca²⁺ influx through receptor-operated Ca²⁺ channels (ROCC) and J_{SOCC} the influx through SOCC. We neglect the Ca²⁺ influx through voltage-operated Ca²⁺ channels (VOCC) because membrane depolarisation plays little role during agonist-induced [Ca²⁺]_i signalling and contraction in ASMC (in contrast to other types of muscle cells, including vascular smooth muscle cells, where action potentials are crucial to contraction) [1,31]. The Ca²⁺ influxes are modelled by:

$$J_{leakin} = \alpha_0, \quad (3a)$$

$$J_{ROCC} = \alpha_1 p, \quad (3b)$$

$$J_{SOCC}(P_{so}) = V_s P_{so}. \quad (3c)$$

where α_0 and α_1 are constants, p is the agonist concentration, V_s is the maximum SOCC flux, and P_{so} represents the fraction of STIM proteins bound to Orai/TRP proteins, i.e. the fraction of activated SOCC. This fraction adapts slowly to changes in c_s , because the diffusion of STIM within the SR membrane is a slow process [32]. We model this phenomenologically by

$$\frac{dP_{so}}{dt} = (P_{so}^\infty(c_s) - P_{so})/\tau_s, \quad (4a)$$

$$P_{so}^\infty(c_s) = \frac{K_s^4}{K_s^4 + c_s^4}. \quad (4b)$$

The steady-state function P_{so}^∞ can be interpreted as the fraction of STIM proteins dissociated from SR Ca²⁺ (as a consequence of store depletion), and thus able to oligomerise and move toward the PM to bind with Orai and/or TRP (see also Discussion). P_{so}^∞ is therefore a decreasing function of [Ca²⁺]_{SR}, which we model by the reverse Hill function Eq. (0b), assuming affinity K_s for [Ca²⁺]_{SR} and Hill coefficient $n_s = 4$ [33].

The total Ca²⁺ flux from the SR into the cytosol is given by

$$J_{rel} = J_{IPR} + J_{RyR} + J_{leakSR}, \quad (8)$$

where J_{IPR} is the Ca²⁺ flux through IP₃ receptors (IPR), J_{RyR} the Ca²⁺ flux through ryanodine receptors (RyR), and J_{leakSR} an unspecified Ca²⁺ leak out of the SR. We use the formulation (e.g., [30]):

$$J_{rel} = (k_{IPR}P_{IPR} + k_{RyR}P_{RyR} + J_{SR})(c_s - c) \quad (9)$$

where k_{IPR} (resp. k_{RyR}) is the maximum rate of Ca²⁺ flow through IPR (resp. RyR). Following [23], the IPR opening probability P_{IPR} is modelled using the Li-Rinzel/Tang et al. reduction of the De Young-Keizer (DYK) model [34–36]:

$$P_{IPR}(c, y) = \left(\frac{pc(1-y)}{(p + K_1)(c + K_5)} \right)^3, \quad (10)$$

where p is the IP₃ concentration, and y is the fraction of inhibited IPR. The latter obeys

$$\frac{dy}{dt} = \Phi_1(c)(1-y) - \Phi_2 y, \quad (11)$$

with

$$\begin{aligned} \Phi_1(c) &= k_2^- \frac{(k_{42}K_2K_1 + K_4p)c}{K_4K_2(K_1 + p)}, \\ \Phi_2 &= k_2^- \frac{p + k_{42}K_3}{K_3 + p}. \end{aligned} \quad (12)$$

The parameters $K_i = k_i^-/k_i^+$ ($i = 1, \dots, 4$) are equilibrium constants for IP₃ and Ca²⁺ binding/unbinding to the IPR; we use the original values from the DYK model [34]. The value of k_2^- is scaled so that the range of [Ca²⁺]_i oscillation frequencies matches the experimental range, with the ratio $k_{42} = k_4^-/k_2^-$ kept constant to the value in ref. [30] (see also Table 1). In the experiments modelled in this work, either RyR play a negligible role, or they are locked open by Rya-Caf treatment (see Results). Hence, we neglect their dynamics and set the fraction of open RyR, P_{RyR} , either to 0 or 1 depending on the experiment considered.

The Ca²⁺ ATP-ases are modelled using the usual expressions (e.g., [30]):

$$J_{PMCA}(c) = V_p \frac{c^2}{K_p^2 + c^2}, \quad J_{SERCA}(c) = V_e \frac{c^2}{K_e^2 + c^2}. \quad (13)$$

We do not model Ca²⁺ pumping into mitochondria explicitly, but acknowledge that a portion of the extrusion process attributed to PMCA might actually be performed by mitochondria uniporters, as these might be activated at average [Ca²⁺]_i as low as 1 μ M [20].

Gathering all expressions, the model is described by:

$$\begin{aligned} \frac{dc}{dt} &= \alpha_0 + \alpha_1 p + V_s P_{so} - V_p \frac{c^2}{K_p^2 + c^2} \\ &\quad + (k_{IPR}P_{IPR}(c, y) + k_{RyR}P_{RyR} + J_{SR})(c_s - c) - V_e \frac{c^2}{K_e^2 + c^2}, \\ \frac{dc_s}{dt} &= \gamma \left(V_e \frac{c^2}{K_e^2 + c^2} - (k_{IPR}P_{IPR}(c, y) + k_{RyR}P_{RyR} + J_{SR})(c_s - c) \right), \\ \frac{dy}{dt} &= \Phi_1(c)(1-y) - \Phi_2 y, \\ \frac{dP_{so}}{dt} &= (P_{so}^\infty(c_s) - P_{so})/\tau_s. \end{aligned} \quad (14)$$

In addition to Eq. (11), we use the following expressions to account for the time needed by drugs to reach full effect:

Table 1. Parameter values used in the model.

Parameter	symbol	value	units	reference
PMCA maximum flux	V_p	7.5	$\mu\text{M/s}$	this work
PMCA affinity	K_p	1.5	μM	0.1–1 [59]
SOCE maximum flux	V_s	1.57	$\mu\text{M/s}$	this work
STIM SR Ca ²⁺ affinity	K_s	50	μM	$\sim c_s^*/2$
SOCE Hill exponent	n_s	4		[33]
SOCE timescale	τ_s	30	s	[32]
Constant leak influx	α_0	0	$\mu\text{M/s}$	$\ll V_s$
Cyt/SR vol. \times buffer effects	γ	5.405		[34,60]
ROCE rate	α_1	0.00105	s^{-1}	this work
SERCA maximum flux	V_e	5	$\mu\text{M/s}$	this work
SERCA affinity	K_e	0.1	μM	0.1–1 [61]
CPA effect timescale	τ_e	30	s	\sim min
IPR rate	k_{IPR}	0.667	s^{-1}	this work
Agonist concentration	\bar{p}	1	μM	this work
Agonist effect timescale	τ_p	30	s	\sim min
SR leak rate	J_{SR}	0.01	s^{-1}	$\ll k_{IPR}$
RyR leak rate (Rya-Caf effect)	K_{RyR}	0.19	s^{-2}	this work
Rya-Caf effect timescale	τ_{SR}	10	s	\sim min
IPR affinity for IP ₃	K_1	0.138	μM	[34]
IPR affinity for Ca ²⁺ (inhib. site)	K_2	1.05	μM	[34]
IPR affinity for IP ₃	K_3	0.943	μM	[34]
IPR affinity for Ca ²⁺ (inhib. site)	K_4	0.144	μM	[34]
IPR affinity for Ca ²⁺ (activ. site)	K_5	0.082	μM	[34]
IPR Ca ²⁺ dissoc. rate (inhib. site)	k_2^-	0.167	s^{-1}	this work
IPR Ca ²⁺ dissoc. rate (inhib. site)	k_4^-	0.138 k_2^-	s^{-1}	[34]

For $\bar{p}=0$ and $k_{RyR}=0$, the equilibrium Ca²⁺ concentrations are $c^*=68.1\text{nM}$ and $c_s^*=158\mu\text{M}$, which are in the physiological ranges [40,41].
doi:10.1371/journal.pone.0069598.t001

$$p(t) = \bar{p}(1 - e^{-t/\tau_p}), \quad (15)$$

$$P_{RyR}(t) = 1 - e^{-t/\tau_{SR}}, \quad (16)$$

$$J_{SERCA}(t) = V_e \frac{c(t)^2}{K_e^2 + c(t)^2} e^{-t/\tau_e}. \quad (17)$$

These equations describe respectively agonist stimulation, Rya-Caf treatment, and SERCA block by CPA (see Results).

Unless otherwise mentioned, parameter values were freely adapted (within physiological ranges when they are known) to account for the experimental results. The values retained are listed in Table 1. The fitting was performed “by hand” (i.e., no algorithmic method was used) within the Mathematica “Manipulate” environment (a useful framework for fitting an ODE model to several experimental results as it enables visualisation of the effect of a parameter change on several ODE integrations almost instantaneously). The code can be made freely available upon request for academic, non-commercial use.

All simulations were run from the same initial condition as in the experiment, which is usually the physiological equilibrium.

Bifurcation diagrams were computed using the numerical continuation software AUTO [37,38].

Results

Accounting for [Ca²⁺]_i dynamics of AMSC in lung slices

Fig. 3A–C shows representative [Ca²⁺]_i dynamics of an ASMC in a human lung slice in response to a three-step experimental protocol [2]. This protocol was originally designed to clamp the [Ca²⁺]_i of ASMC, in order to study independently the effects of agonist and [Ca²⁺]_i on airway contraction [28]. The slice is first stimulated with agonist (histamine), to verify its viability (Fig. 3A). This induces [Ca²⁺]_i oscillations. Agonist is then washed from the slice, and a Rya-Caf treatment is applied (Fig. 3B). This creates a permanent Ca²⁺ leak through RyR, because caffeine opens RyR and ryanodine locks them open irreversibly. If this Ca²⁺ leak is large enough, it keeps the SR empty and prevents any further change in [Ca²⁺]_i, unless extracellular Ca²⁺ is modified. The effectiveness of the treatment is confirmed by the second application of agonist (Fig. 3C): no further [Ca²⁺]_i increase is triggered, showing that [Ca²⁺]_i is clamped. It is important to emphasise that these results are not specific to histamine stimulation of human lung slices: similar results have been obtained in mouse and rat lung slices with methylcholine (Fig. 6 in ref. [29], Figs. 5B and 6C–D in ref. [28]).

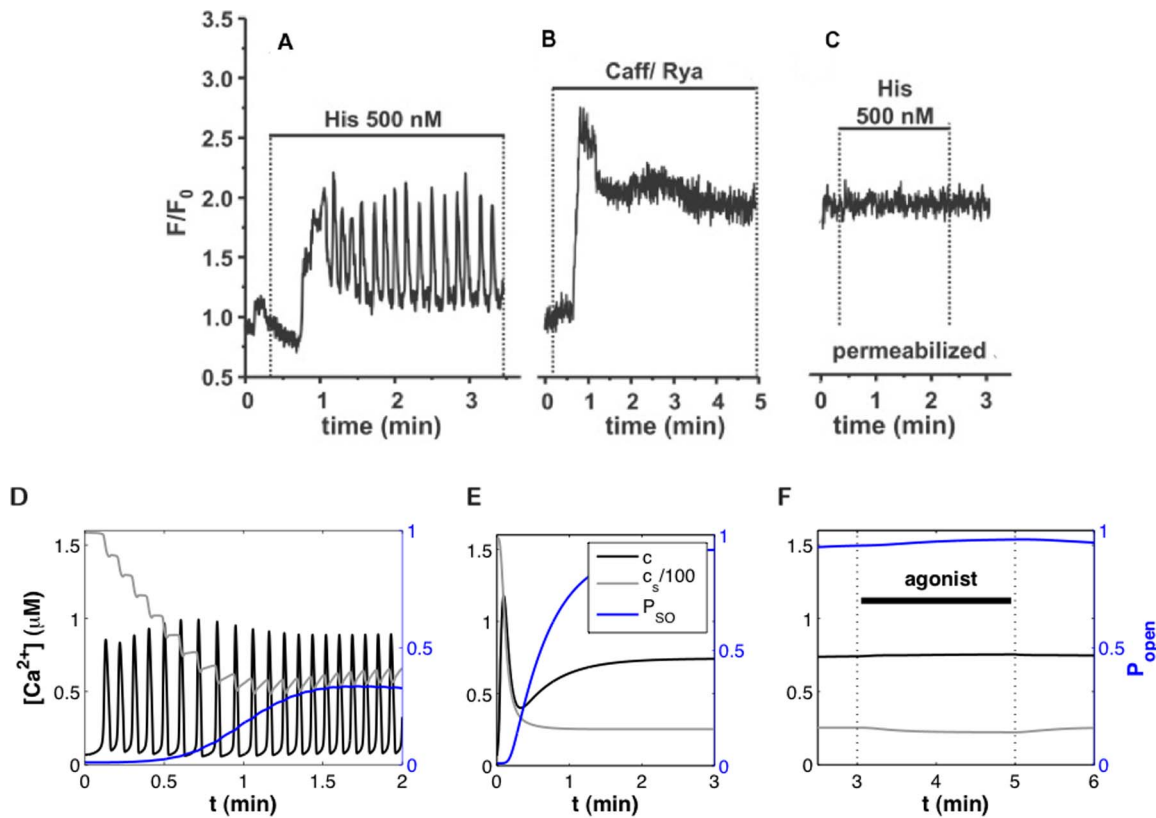


Figure 3. $[\text{Ca}^{2+}]_i$ dynamics in ASMC: experiment and model. (A)–(C): Fluorescence imaging of $[\text{Ca}^{2+}]_i$ dynamics in an ASMC within a human lung slice, during the following 3-step experiment: (A) Agonist stimulation, (B) Rya-Caf treatment, and (C) second agonist stimulation. Following the irreversible Rya-Caf treatment in (B), agonist stimulation (C) is no longer able to elicit Ca^{2+} oscillations, nor does it perturb the new elevated $[\text{Ca}^{2+}]_i$ equilibrium. Reprinted from [2] under a CC BY license, with permission of the American Thoracic Society, original copyright 2010. Cite: Ressemeyer et al. / 2010/Am J Respir Cell Mol Biol/43/179–191. Official journal of the American Thoracic Society. This modified figure is based on the original figure available from www.atsjournals.org. (D)–(F): Simulations of the experiments in (A)–(C) using Eqs. 114–12 and the parameter values in Table 1. The evolution of $[\text{Ca}^{2+}]_i$, $[\text{Ca}^{2+}]_{SR}$, and P_{so} (fraction of open SOCC) are shown (cf. legend in (E)). doi:10.1371/journal.pone.0069598.g003

The mathematical model enables the deduction of valuable information from the experimental results. First, from Eq. (14), the new, elevated, $[\text{Ca}^{2+}]_i$ equilibrium reached after Rya-Caf treatment satisfies:

$$J_{PMCA}(c^*) = J_{leakin} + J_{ROCC}(p) + J_{SOCC}(c_s^*), \quad (13a)$$

$$J_{SERCA}(c^*) = (k_{IPR}P_{IPR}(c^*, c_s^*) + k_{RyR}P_{RyR} + J_{SR})(c_s^* - c^*), \quad (13b)$$

where c^* and c_s^* are respectively the equilibrium $[\text{Ca}^{2+}]_i$ and $[\text{Ca}^{2+}]_{SR}$. An important consequence of (18) is that, in the absence of SOCE, c^* depends only on the Ca^{2+} fluxes through the PM. This may seem surprising, as any increase in Ca^{2+} flux out of the SR (J_{rel} in Eq. (1)) is expected to increase $[\text{Ca}^{2+}]_i$. However, the equilibrium equation (18) tells us that such an increase would only be transient (because the PMCA pumping rate is an increasing function of $[\text{Ca}^{2+}]_i$), unless there is a concomitant permanent increase in Ca^{2+} influx through the PM. Hence, the persistence of an elevated $[\text{Ca}^{2+}]_i$ means that a permanent SOCE has been elicited (as SOCE is the only Ca^{2+} influx capable of increase upon Rya-Caf treatment). Moreover, the model indicates that ROCE is negligible after Rya-Caf treatment. Indeed, if it was not, the

addition of agonist would increase c^* via the increase in J_{ROCC} . Hence, we assume that the ROCE rate α_1 is small (see Table 1 and Discussion).

Results of “hand-fitting” the model to the experimental results are shown in Figs. 3D–F and Fig. 4, with the corresponding parameter values listed in Table 1. The model reproduces (i) the agonist-induced Ca^{2+} oscillations, (ii) the similar magnitudes of the new equilibrium $[\text{Ca}^{2+}]_i$ in Fig. 3B and the amplitude of the oscillations in Fig. 3A, and (iii) the negligible effect of agonist stimulation after Rya-Caf treatment. Agonist-induced Ca^{2+} oscillations were simulated with $P_{RyR} = 0$ because RyR appear to play a negligible role during agonist-induced Ca^{2+} oscillations [2,39]. On the other hand, the response to Rya-Caf was simulated with $P_{RyR} = 1$ since the treatment locks open the RyR. We did not attempt to reproduce the magnitude of the initial spike response to Rya-Caf treatment relative to that of the subsequent $[\text{Ca}^{2+}]_i$ plateau (Fig. 3B) because the fluorescent dye used in the experiments saturates rapidly with $[\text{Ca}^{2+}]_i$. Parameter values were also adjusted to yield physiological Ca^{2+} equilibrium concentrations ($c \sim 0.1 \mu\text{M}$ [40] and $c_s \sim 500 \mu\text{M}$ [41]), realistic $[\text{Ca}^{2+}]_i$ oscillation amplitude ($\sim 1 \mu\text{M}$), and to reproduce the range of $[\text{Ca}^{2+}]_i$ oscillation frequencies observed in human lung slices as a function of agonist (0.5–11/min [2]). More detail

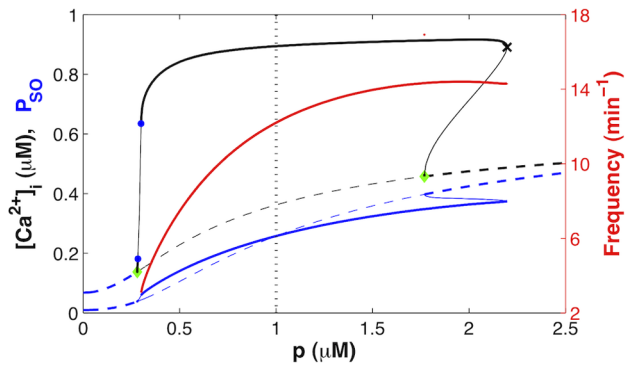


Figure 4. Ca^{2+} dynamics as a function of agonist concentration. Dashed curves represent steady-states (constant Ca^{2+} levels); solid curves, periodic solutions (Ca^{2+} oscillations). The maximum $[\text{Ca}^{2+}]_i$ (black) and the maximum fraction of open SOCC (blue) during one solution period are plotted as ordinates. The red curve (right y-axis) shows the frequency of the Ca^{2+} oscillations on the main stable segment (from the upper blue dot to the black cross), which fits the experimental range in human [2]. The stable solutions are represented as thick lines and unstable solutions as thin lines. The green diamonds represent Hopf bifurcations, the black cross, a saddle-node bifurcation, and the blue dots, period-doubling points. Period-doubled branches are not shown because they extend only over a tiny range of p values; moreover it is likely that the deterministic description of Ca^{2+} oscillations fails at these low agonist concentrations (see Discussion). The vertical dotted line indicates the value of p used in Fig. 3 (Table 1). doi:10.1371/journal.pone.0069598.g004

on the parameter estimation procedure is given in Supporting Information S1.

Fig. 4 shows the bifurcation diagram of the model as a function of agonist concentration. Periodic solutions (i.e., Ca^{2+} oscillations) arise through a Hopf bifurcation, and disappear through a saddle-node bifurcation of limit cycles. A second Hopf bifurcation is present on the steady-state branch, and is associated with a region of bistability between the steady-state and the periodic solution at the right of the bifurcation diagram. It is not known whether such bistability occurs in reality. It should also be noted that the steady-state $[\text{Ca}^{2+}]_i$ increases with agonist concentration, as is expected (e.g., [30]). This increase is provided by SOCE in our model. Indeed, the Ca^{2+} flux through

IPR increases with agonist, so that store depletion increases as well.

Effect of SOCE regulation on agonist-induced Ca^{2+} oscillations

SOCE is the main Ca^{2+} influx in the model, as ROCE is negligible (see above) and the Ca^{2+} leak influx is (by definition) small. Fig. 3D shows that while SOCE is almost zero at physiological equilibrium (initial condition), it substantially increases during agonist-induced Ca^{2+} oscillations (final condition; see also Fig. 4), due to significant SR Ca^{2+} depletion. Therefore, changes in SOCE can be expected to have a substantial effect on Ca^{2+} oscillations. This is quantified in Fig. 5, where the amplitude and frequency of Ca^{2+} oscillations are plotted as a function of (a) the maximum SOCE rate, V_s , and (b) STIM affinity for Ca^{2+} , K_s (the $[\text{Ca}^{2+}]_{SR}$ at which half SOCC are open). It is found that the $[\text{Ca}^{2+}]_i$ oscillation frequency varies as much with V_s and K_s at fixed agonist concentration (Fig. 5) as it varies with agonist concentration at fixed SOCE parameters (Fig. 4). Moreover, a too big departure from the “normal” values (dotted lines, Table 1) leads to the extinction of the Ca^{2+} oscillations (via a Hopf bifurcation to the left, and a saddle-node to the right, of the bifurcation diagrams in Figs. 5A–B). These results are not very surprising to the extent that Ca^{2+} oscillations are expected to depend crucially on Ca^{2+} influx (e.g., [42]). However, they suggest that SOCE could play a role in AHR since (i) $[\text{Ca}^{2+}]_i$ oscillations mediate ASMC contraction, and (ii) SOCE up-regulation (which increases $[\text{Ca}^{2+}]_i$ oscillation frequency) can be triggered by inflammatory mediators commonly found in asthma [9,11,24].

Partial inhibition of SERCA by CPA

We now apply the model to experimental data from mouse lung slices showing an attempt to clamp $[\text{Ca}^{2+}]_i$ with the SERCA blocker CPA, instead of Rya-Caf treatment (Fig. 6). After inducing Ca^{2+} oscillations with agonist, CPA is applied in the presence of agonist (for faster emptying of the SR than CPA alone) and causes a gradual damping of the Ca^{2+} oscillations, together with a rise of the $[\text{Ca}^{2+}]_i$ baseline, until the oscillations become undistinguishable from fluctuations around an elevated steady $[\text{Ca}^{2+}]_i$ mean. Because CPA is believed to inhibit SERCA, the assumption, at this stage of the experiment, is that the SR is empty and SOCE fully

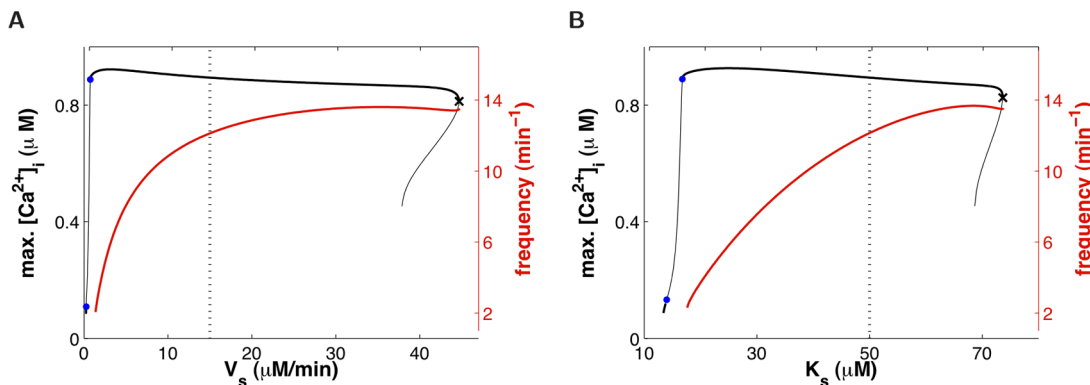


Figure 5. Influence of SOCE on agonist-induced $[\text{Ca}^{2+}]_i$ oscillations. Amplitude (black) and frequency (red) of Ca^{2+} oscillations as a function of (A) SOCE maximum rate, V_s , and (B) STIM affinity for SR Ca^{2+} , K_s . Dotted lines indicate the “normal” parameter values (Table 1, Figs. 3D–F). As in Fig. 4, only the frequency of the large-amplitude stable Ca^{2+} oscillations is shown. doi:10.1371/journal.pone.0069598.g005

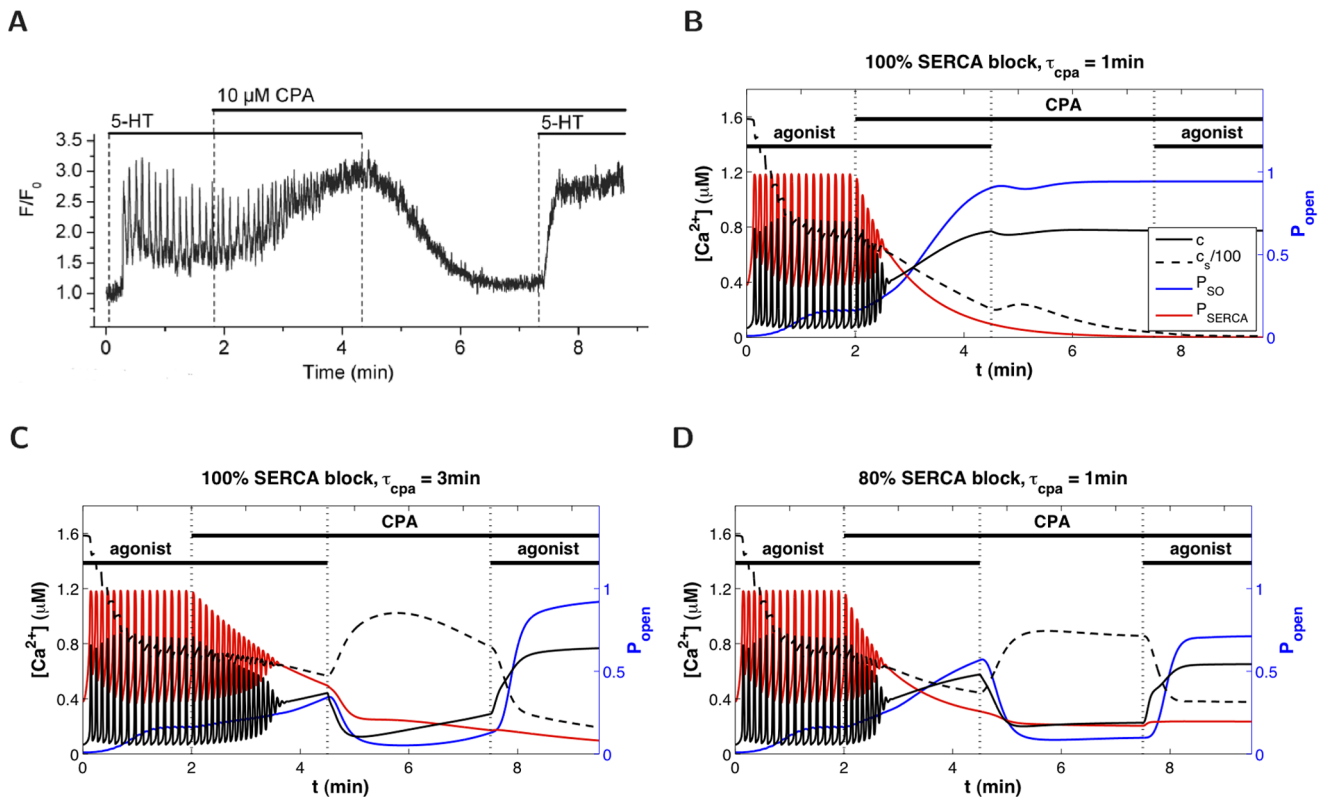


Figure 6. Effect of CPA on $[\text{Ca}^{2+}]_i$ dynamics. (A) Fluorescence imaging of $[\text{Ca}^{2+}]_i$ in ASMC of a mouse lung slice treated with agonist and CPA. Agonist removal leads to $[\text{Ca}^{2+}]_i$ decrease. (B–D) Model simulations of the experiments shown in (A), assuming that (B) CPA quickly blocks the SERCA, (C) CPA slowly blocks the SERCA, (D) CPA partially blocks the SERCA but reaches maximum strength rather quickly. Black solid and dashed curves (left y-axis) represent respectively $[\text{Ca}^{2+}]_i$ and $[\text{Ca}^{2+}]_{\text{SR}}$; blue and red curves (right y-axis) show respectively the fraction of open SOCC and the fraction of operating SERCA (that is, $P_{\text{SERCA}} = J_{\text{SERCA}}/V_{\text{er}}$, where J_{SERCA} is given by Eq. (0c)). doi:10.1371/journal.pone.0069598.g006

active. However, when agonist is removed (CPA remains), $[\text{Ca}^{2+}]_i$ falls. When agonist is reapplied, $[\text{Ca}^{2+}]_i$ increases. These $[\text{Ca}^{2+}]_i$ responses to agonist addition and removal are not observed when SOCE is evoked by Rya-Caf treatment. According to our model (Eq.(18)), the decrease in $[\text{Ca}^{2+}]_i$ upon agonist removal indicates that SOCE does not remain activated, i.e. that the SR refills with Ca^{2+} . This suggests that the SERCA are not completely blocked by CPA, as illustrated by the simulations in Fig. 6B–D. If CPA was to fully block the SERCA (Fig. 6B), $[\text{Ca}^{2+}]_i$ would not decrease upon agonist removal. If $[\text{Ca}^{2+}]_i$ falls, it must be because either CPA requires a longer time than that used in the experiment to fully block the SERCA (Fig. 6C), or CPA achieves only partial block of the SERCA (Fig. 6D).

Experiments of longer duration were performed to test the model predictions. Fig. 7A shows that if CPA is applied in the presence of agonist for 5 minutes, followed by CPA only for a further 10 minutes, $[\text{Ca}^{2+}]_i$ still returns to the original equilibrium level when agonist is removed, and remains low until agonist is reintroduced. This suggests that the explanation in Fig. 6C can be rejected, otherwise the longer exposure to CPA should yield a result similar to Fig. 6B. The inability of CPA to fully empty the SR of Ca^{2+} is confirmed by Fig. 7B, where extracellular calcium is removed before agonist is applied a second time, to prevent any potential ROCE. The Ca^{2+} response induced can thus be unambiguously attributed to Ca^{2+} release from the SR.

Hence, our combined modelling and experimental study indicates that CPA blocks only partially the SERCA of ASMC

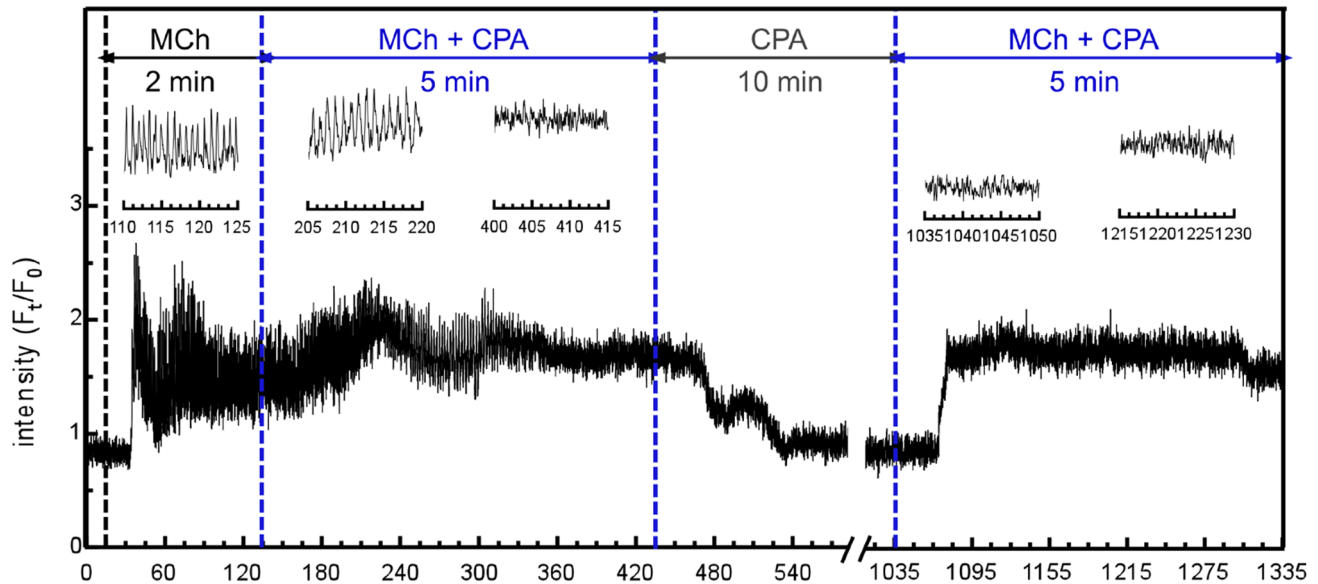
in lung slices (scenario simulated in Fig. 6D). This is a potentially important result given the wide use of CPA in cell biology to study SOCE. We note that Figs. 6A and 7 could also be explained by a model assuming that ROCE, instead of SOCE, is the main Ca^{2+} influx (e.g., [23]). However, such a model would fail to explain the outcome of Rya-Caf treatment in human and mouse lung slices (both the persistent elevated $[\text{Ca}^{2+}]_i$ in the absence of agonist, and the absence of effect of agonist on this elevated $[\text{Ca}^{2+}]_i$). In contrast, our model, constructed to account for both agonist-induced oscillations and Rya-Caf treatment, explains the CPA results without requiring any modification. Its prediction holds provided CPA is not a 100% efficient SERCA blocker, and this hypothesis is supported by the experimental data in Fig. 7.

Discussion

Modelling SOCE

Our mathematical model accounts for the two main properties of SOCE: 1) SOCE is an increasing function of Ca^{2+} store depletion, and 2) it activates slowly upon store depletion. While the mechanisms of SOCE activation are rather well understood [14,32], the mechanisms of SOCE termination remain less clear [43,44]. Hence, we do not explicitly distinguish between SOCE activation and inactivation in the model, and use a single parameter K_s for STIM affinity for SR Ca^{2+} and a single time constant τ_s for the slow adaptation to changes in $[\text{Ca}^{2+}]_{\text{SR}}$. This is also justified by the fact that most experimental data available on

A



B

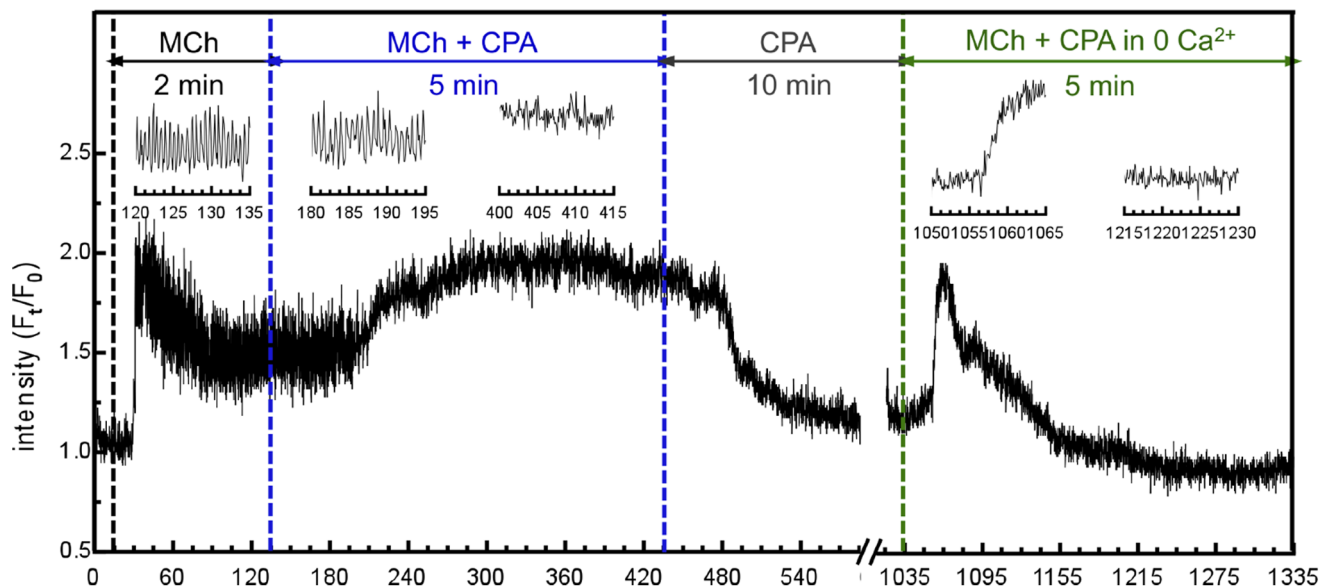


Figure 7. Experimental evidence that CPA does not fully empty the SR of ASM cells. Tests of the model predictions shown in Fig. 6B–D, performed with mouse lung slices. (A) Significantly longer exposure to agonist+CPA and to CPA than in Fig. 6A still fails to maintain SOCE. (B) Same experiment as in (A) except that extracellular Ca^{2+} is removed before agonist is applied a second time, confirming the residual presence of Ca^{2+} in the SR and hence the partial efficacy of CPA to inhibit SERCA (scenario of Fig. 6D). (Insets show magnifications of selected time windows). doi:10.1371/journal.pone.0069598.g007

SOCE come from a category of SOCC called CRACC (Ca^{2+} - release-activated Ca^{2+} channels), which are highly selective to Ca^{2+} , while there is evidence that SOCE in ASM cells (and in other cells) occurs at least in part through non-selective Ca^{2+} channels (NSCC). It could be that the latter operate somewhat differently from CRACC in response to store depletion or refilling.

Our description of SOCE slow activation upon store depletion is continuous, which is easy to handle computationally, and compatible with experimental knowledge. Indeed, it is reasonable

to assume that a small fraction of STIM proteins reside in close proximity to the PM, and may thus bind Orai quickly upon store depletion. Hence, a weak SOCE is likely to occur almost instantaneously upon store depletion, rendering unnecessary to introduce a finite activation delay in the model via a delay-differential equation.

We are aware of only few prior works on Ca^{2+} dynamics that include a mathematical description of SOCE, all of which are ODE models [15–18]. The first two were published before the molecular basis for SOCE was established. The latter two works

include more realistic descriptions of SOCE, but none of them accounts for the slow translocation of oligomerised STIM to the PM, while it is recognised as the rate-limiting event for SOCE activation [32]. Ong *et al.* however assume a slow diffusion of Ca^{2+} between internal SR and superficial SR (modelled as distinct compartments exchanging Ca^{2+}), with SOCE being triggered by peripheral SR depletion [17]. Liu *et al.* explicitly model both SR Ca^{2+} dissociation from STIM and binding of STIM to Orai. Both models are used to study transient $[\text{Ca}^{2+}]_i$ responses only; $[\text{Ca}^{2+}]_i$ oscillations are not considered. Prior models of Ca^{2+} dynamics specific to ASMC did not include SOCE, while we have shown that this is necessary to account for several experimental results obtained with lung slices. The work of Haberichter *et al.* [19] focused on the influence of the different IPR isoforms on Ca^{2+} signalling in ASMC. Brumen *et al.* studied the influence of the total Ca^{2+} content on the nature (damped or sustained) and frequency of agonist-induced Ca^{2+} oscillations [21]. Roux *et al.* did not model Ca^{2+} oscillations, but transient Ca^{2+} responses to caffeine [20]. Finally, the model by Wang *et al.* [23] addressed the different contributions of IPR and RyR to agonist-induced and KCl-induced Ca^{2+} oscillations in ASMC.

From the mathematical point of view, the fact that SOCE is an explicit function of store Ca^{2+} renders the models of Ca^{2+} dynamics including this influx qualitatively different from those which do not, as SOCE couples the homogenous steady-state $[\text{Ca}^{2+}]_i$ to $[\text{Ca}^{2+}]_{SR}$ (Eq. (18)). This property is essential for the predictions of our model (in particular, the persistence of an elevated $[\text{Ca}^{2+}]_i$ upon sustained store depletion in the absence of agonist). On the other hand, whether SOCE is an instantaneous or delayed function of $[\text{Ca}^{2+}]_{SR}$ appears to have little effect on our results.

SOCE vs. ROCE

While Fig. 3C (as well as Fig. 6 in ref. [29], Figs. 5B and 6C-D in ref. [28]) shows that no ROCE is elicited by agonist following Rya-Caf treatment, it does not imply that ROCE cannot play a substantial role during other, more physiological, conditions, such as agonist-induced Ca^{2+} oscillations. It could be that ROCE is inhibited at the large $[\text{Ca}^{2+}]_i$ levels induced by SOCE activation following Rya-Caf treatment. Instead of assuming the existence of an inactivation process at large $[\text{Ca}^{2+}]_i$, we assumed, for simplicity, that ROCE is negligible in the model. This approach enabled us to show that Ca^{2+} influx through SOCC is sufficient to sustain agonist-induced $[\text{Ca}^{2+}]_i$ oscillations, and to explain the experimental results obtained with CPA, although the latter could be interpreted as evidence for ROCE at first sight. The fact that there appears to be no selective blocker for SOCE and ROCE makes it difficult to evaluate experimentally the respective contributions of the two Ca^{2+} influxes during physiological conditions. These magnitudes are probably also cell-type dependent. Such issues explain the persistence of the controversy regarding SOCE and ROCE [45–48]. An informative experiment would be to stimulate ASMC using flash photolysis of caged IP_3 instead of agonist stimulation. Indeed, as IP_3 does not induce ROCE, SOCE should be the essential Ca^{2+} influx left. By comparing the responses to IP_3 stimulation in the presence and in the absence of extracellular calcium, one could then deduce the importance of SOCE in physiological conditions.

Efficacy of CPA

CPA is widely used as a SERCA blocker, having the advantage over Thapsigargin (Tg) of being reversible, and probably less toxic.

Both have been used extensively to study SOCE in different cell types (e.g., [25–27,43,49]). Although our work indicates that CPA does not fully block the SERCA in intact tissue such as lung slices, it does not imply that CPA should not be used experimentally to induce SOCE. Indeed, CPA might still cause substantial SOCE activation in the presence of agonist. However, our results indicate that CPA is not a good mean to fully empty Ca^{2+} stores, and care should be taken in interpreting the experimental results of its application. We suggest that a combined Rya-Caf treatment is a more reliable way to induce a permanent large SR depletion (Fig. 3B, C). There is evidence that Tg is an efficient SERCA blocker in cell lines such as Hela cells [43], but we have not addressed the effect of Tg on ASMC in lung slices in this study.

Modelling IPR

In this work, we followed the approach of Wang *et al.* [23], in that we have used one of the simplest models of IPR Ca^{2+} release, namely the Li-Rinzel/Tang *et al.* reduction of the DYK ODE model [34–36]. This category of IPR model produces agonist-induced Ca^{2+} oscillations characterised by significant SR Ca^{2+} depletion (Fig. 3D and [23]), hence the possibility of SOCE being activated during such Ca^{2+} oscillations. This property might be model-dependent, however there is evidence that the SR is actually depleted to some extent during agonist-induced Ca^{2+} oscillations in ASMC. Indeed, the absence of effect of ryanodine during agonist-induced oscillations can be explained by the average level of $[\text{Ca}^{2+}]_{SR}$ being too low for RyR activation [1,23]. However, the respective $[\text{Ca}^{2+}]_{SR}$ “thresholds” for SOCE and RyR activation are experimentally unknown. In this work, the SOCE activation threshold was deduced from fitting the model simultaneously to Fig. 3A and Figs. 3B–C.

Finally, we note that our whole-cell $[\text{Ca}^{2+}]_i$ model would likely not benefit from using a recent Markov model of an IPR (e.g., [50–52]), because these models are based on steady-state data only (i.e., single-channel opening and closing times in stationary Ca^{2+} and IP_3) and typically miss the long inactivation timescale which was included “ad hoc” in the first IPR models to reproduce the observed behavior at the cell level (i.e., $[\text{Ca}^{2+}]_i$ oscillations upon agonist stimulation).

Limitations of the whole-cell model

As we are essentially interested in $[\text{Ca}^{2+}]_i$ responses of ASMC at the cell level, we have described Ca^{2+} dynamics via a deterministic ODE model. The scope of this model is, however, somewhat limited for the following reasons.

First, there is evidence that IPR are not homogeneously distributed on the SR membrane of cells, but are found as dense clusters. This channel clustering is especially patent upon stimulation by low agonist concentrations, for which local, stochastic Ca^{2+} releases may not propagate to neighboring clusters, resulting in spatially isolated, unsynchronised Ca^{2+} releases, called “puffs”. At higher agonist concentrations, the frequency of these puffs increases, allowing Ca^{2+} releases from close sites to accumulate and propagate further away. This triggers, via CICR, the firing of more distant clusters, and results in Ca^{2+} waves propagating repeatedly throughout the cytosol. These waves usually appear as Ca^{2+} oscillations at the whole-cell level. While Ca^{2+} waves are indeed associated with $[\text{Ca}^{2+}]_i$ oscillations in ASMC [1], it has, so far, been impossible to detect Ca^{2+} puffs. This could arise from a less clustered distribution of IPR in ASMC, compared to the larger cells (oocytes and Hela cells) where puffs have been characterised. On the other hand,

Ca²⁺ “sparks”, the equivalent of Ca²⁺ puffs but mediated by RyR, have been detected in ASMC [1], which supports a clustered distribution of RyR. In this study, we did not attempt to consider these spatial/stochastic aspects of the Ca²⁺ signals. Our model is thus less reliable at low agonist concentrations.

Second, cytoplasmic microdomains often exist between cell organelles (e.g., between peripheral SR and the plasma membrane, between the SR and mitochondria), out of which [Ca²⁺]_i cannot diffuse easily. These have consequences for SOCE dynamics. Indeed, it has been reported that upon store depletion, SERCA can colocalise with STIM proteins, in proximity to the PM [49,53]. As a consequence, if SOCE is slow enough, the SR can refill with Ca²⁺ without a concomitant increase in bulk [Ca²⁺]_i [49]. Upon large SOCE, this is no longer the case; however, mitochondria prevent the local Ca²⁺ increase to become too large by pumping Ca²⁺ from the subplasmalemmal space and releasing it deeper in the cytoplasm, where it can be absorbed by other SERCA [49]. These spatial effects cannot be accounted for by our current non-compartmentalised model.

Finally, Ca²⁺ dynamics are modified by Ca²⁺ buffers in the cytosol and SR, which bind 99% of the free Ca²⁺. While the effect of fast, linear buffers can be taken into account by a global rescaling of Ca²⁺ fluxes (see Methods), this is not the case for high affinity buffers, in particular fluorescent dye indicators. Including such buffers in an ODE model of [Ca²⁺]_i dynamics leads to suppression of [Ca²⁺]_i oscillations, because the buffer affinity is close to the amplitude of whole-cell [Ca²⁺]_i oscillations. In reality, [Ca²⁺]_i reaches much higher levels locally upon IPR opening, so that the buffers become saturated and cannot prevent Ca²⁺ oscillations. Again, this would have to be accounted for by a spatial model of Ca²⁺ dynamics.

Future work

Although RyR dynamics play a role only during the initial phases of agonist-induced Ca²⁺ oscillations and Rya-Caf treatment, the interaction between RyR and IPR may become important in other situations, such as drug-induced RyR sensitisation. We plan to extend our model to these dynamics.

Since our work is part of a broader effort to improve the understanding of airway hyper-responsiveness and remodelling via mathematical modelling [54–57], we also intent to model the interaction of ASMC Ca²⁺ signalling with other aspects of lung dynamics. Although mathematical models of ASM contraction have previously been developed [54,55,58], modelling of other

signalling pathways, such as inflammation and proliferation, is, to our knowledge, still in its infancy.

Additionally, experimental studies of ASMC inflammation and proliferation in conjunction with [Ca²⁺]_i imaging in lung slices would be desirable. While such studies have been carried out with cultured ASMC [3–5,9–12], they do not provide individual [Ca²⁺]_i dynamics; moreover, cultured ASMC often exhibit a different phenotype from ASMC in intact tissues.

Conclusions

The inclusion of SOCE in our mathematical model of Ca²⁺ dynamics in ASMC enables a better understanding of the experimental physiology of lung slices. It shows that the different abilities of CPA and Rya-Caf treatment to clamp the [Ca²⁺]_i of ASMC can be explained by their different ability to invoke SOCE. The model predicts that CPA, in contrast with Rya-Caf treatment, is unable to empty the SR because of its inefficiency to fully inhibit the SERCA. Furthermore, by accounting for both agonist-induced Ca²⁺ oscillations and SOCE activation by SR Ca²⁺ depletion, the model shows that SOCE can be a major determinant of the frequency of agonist-induced Ca²⁺ oscillations. Because this frequency of the Ca²⁺ oscillations regulates airway contraction, the model suggests a role for increased SOCE in AHR, a correlation consistent with SOCE up-regulation under inflammatory conditions typical of asthma. These predictions underscore the synergistic role for mathematical modeling in medical research.

Supporting Information

Supporting Information S1 Details of the parameter estimation procedure.

(PDF)

Acknowledgments

We thank Ruediger Thul, Charlotte Billington and Ian Hall for fruitful discussions.

Author Contributions

Conceived and designed the experiments: HC MJS JFPZ XT JS. Performed the experiments: XT JFPZ MJS. Analyzed the data: HC MJS XT JFPZ BSB JS. Contributed reagents/materials/analysis tools: HC MJS XT JFPZ JS. Wrote the paper: HC BSB MJS.

References

- Perez JF, Sanderson MJ (2005) The frequency of calcium oscillations induced by 5-HT, ACH, and KCl determine the contraction of smooth muscle cells of intrapulmonary bronchioles. *J Gen Physiol* 125: 535–53.
- Ressmeyer AR, Bai Y, Delmotte PF, Uy KF, Thistlethwaite P, et al. (2010) Human airway contraction and formoterol-induced relaxation is determined by Ca²⁺ oscillations and Ca²⁺ sensitivity. *Am J Respir Cell Mol Biol* 43: 179–91.
- Sweeney M, McDaniel SS, Platoshyn O, Zhang S, Yu Y, et al. (2002) Role of capacitative Ca²⁺ entry in bronchial contraction and remodeling. *J Appl Physiol* 92: 1594–602.
- Mahn K, Hirst SJ, Ying S, Holt MR, Lavender P, et al. (2009) Diminished sarco/endoplasmic reticulum Ca²⁺ ATPase (SERCA) expression contributes to airway remodelling in bronchial asthma. *PNAS* 106: 10775–80.
- Zou JJ, Gao YD, Geng S, Yang J (2011) Role of STIM1/Orai1-mediated store-operated Ca²⁺ entry in airway smooth muscle cell proliferation. *J Appl Physiol* 110: 1256–63.
- Gerthoffer WT (1991) Regulation of the contractile element of airway smooth muscle. *Am J Physiol Lung Cell Mol Physiol* 5: L15–L28.
- Janney PA (1994) Phosphoinositides and calcium as regulators of cellular actin assembly and disassembly. *Annu Rev Physiol* 56: 169–91.
- Herrera AM, Kuo KH, Seow CY (2002) Influence of calcium on myosin thick filament formation in intact airway smooth muscle. *Am J Physiol Cell Physiol* 282: C310–6.
- White TA, Xue A, Chini EN, Thompson M, Sieck GC, et al. (2006) Role of transient receptor potential C3 in TNF-alpha-enhanced calcium influx in human airway myocytes. *Am J Respir Cell Mol Biol* 35: 243–51.
- Moynihan B, Toloczko B, Michoud MC, Tamaoka M, Ferraro P, et al. (2008) MAP kinases mediate interleukin-13 effects on calcium signaling in human airway smooth muscle cells. *Am J Physiol Lung Cell Mol Physiol* 295: L171–7.
- Sieck GC, White TA, Thompson MA, Pabelick CM, Wylam ME, et al. (2008) Regulation of store-operated Ca²⁺ entry by CD38 in human airway smooth muscle. *Am J Physiol Lung Cell Mol Physiol* 294: L378–85.
- Sathish V, Thompson MA, Bailey JP, Pabelick CM, Prakash YS, et al. (2009) Effect of proinflammatory cytokines on regulation of sarcoplasmic reticulum Ca²⁺ reuptake in human airway smooth muscle. *Am J Physiol Lung Cell Mol Physiol* 297: L26–34.
- Putney JW (1986) A model for receptor-regulated calcium entry. *Cell Calcium* 7: 1–12.

14. Roos J, DiGregorio PJ, Yeromin AV, Ohlsen K, Lioudyno M, et al. (2005) STIM1, an essential and conserved component of store-operated Ca²⁺ channel function. *J Cell Biol* 169: 435–45.
15. Wiesner TF, Berk BC, Nerem RM (1996) A mathematical model of cytosolic calcium dynamics in human umbilical vein endothelial cells. *Am J Physiol Cell Physiol* 270: C1556–C1569.
16. Kowalewski JM, Uhlén P, Kitano H, Brismar H (2006) Modeling the impact of store-operated Ca²⁺ entry on intracellular Ca²⁺ oscillations. *Math Biosci* 204: 232–49.
17. Ong HL, Liu X, Tsaneva-Atanasova K, Singh BB, Bandyopadhyay BC, et al. (2007) Relocalization of STIM1 for activation of store-operated Ca²⁺ entry is determined by the depletion of subplasma membrane endoplasmic reticulum Ca²⁺ store. *J Biol Chem* 282: 12176–85.
18. Liu W, Tang F, Chen J (2010) Designing Dynamical Output Feedback Controllers for Store-operated Ca²⁺ Entry. *Math Biosci* 228: 110–118.
19. Haberichter T, Roux E, Marhl M, Mazat JP (2002) The influence of different InsP3 receptor isoforms on Ca²⁺ signaling in tracheal smooth muscle cells. *Bioelectrochemistry* 57: 129–38.
20. Roux E, Marhl M (2004) Role of sarcoplasmic reticulum and mitochondria in Ca²⁺ removal in airway myocytes. *Biophys J* 86: 2583–95.
21. Brumen M, Fajmut A, Dobovišek A, Roux E (2005) Mathematical Modelling of Ca²⁺ Oscillations in Airway Smooth Muscle Cells. *J Biol Phys* 31: 515–524.
22. Roux E, Noble PJ, Noble D, Marhl M (2006) Modelling of calcium handling in airway myocytes. *Prog Biophys Mol Biol* 90: 64–87.
23. Wang IY, Bai Y, Sanderson MJ, Sneyd J (2010) A mathematical analysis of agonist- and KCl- induced Ca²⁺ oscillations in mouse airway smooth muscle cells. *Biophys J* 98: 1170–81.
24. Gao YD, Zou JJ, Zheng JW, Shang M, Chen X, et al. (2010) Promoting effects of IL-13 on Ca²⁺ release and store-operated Ca²⁺ entry in airway smooth muscle cells. *Pulm Pharmacol Ther* 23: 182–9.
25. Ay B, Prakash YS, Pabelick CM, Sieck GC (2004) Store-operated Ca²⁺ entry in porcine airway smooth muscle. *Am J Physiol Lung Cell Mol Physiol* 286: L909–17.
26. Peel SE, Liu B, Hall IP (2006) A key role for STIM1 in store-operated calcium channel activation in airway smooth muscle. *Respir Res* 7: 119.
27. Peel SE, Liu B, Hall IP (2008) ORAI and store-operated calcium in human airway smooth muscle cells. *Am J Respir Cell Mol Biol* 38: 744–9.
28. Bai Y, Sanderson MJ (2006) Modulation of the Ca²⁺ sensitivity of airway smooth muscle cells in murine lung slices. *Am J Physiol Lung Cell Mol Physiol* 291: L208–21.
29. Bai Y, Sanderson MJ (2009) The contribution of Ca²⁺ signaling and Ca²⁺ sensitivity to the regulation of airway smooth muscle contraction is different in rats and mice. *Am J Physiol Lung Cell Mol Physiol* 296: L947–58.
30. Keener J, Sneyd J (2008) *Mathematical physiology*, second edition. Springer.
31. Janssen IJ (2002) Ionic mechanisms and Ca²⁺ regulation in airway smooth muscle contraction: do the data contradict dogma? *Am J Physiol Lung Cell Mol Physiol* 282: L1161–78.
32. Liou J, Fivaz M, Inoue T, Meyer T (2007) Live-cell imaging reveals sequential oligomerization and local plasma membrane targeting of stromal interaction molecule 1 after Ca²⁺ store depletion. *PNAS* 104: 9301–6.
33. Luik R, Wang B, Prakriya M, Wu M, Lewis R (2008) Oligomerization of STIM1 couples ER calcium depletion to CRAC channel activation. *Nature* 454: 538–542.
34. De Young GW, Keizer J (1992) A single-pool inositol 1, 4, 5-trisphosphate-receptor-based model for agonist-stimulated oscillations in Ca²⁺ concentration. *PNAS* 89: 9895–9899.
35. Li Y, Rinzel J (1994) Equations for InsP3 receptor-mediated [Ca²⁺]_i oscillations derived from a detailed kinetic model: a Hodgkin-Huxley like formalism. *J Theor Biol* 166: 461–473.
36. Tang Y, Stephenson JL, Othmer HG (1996) Simplification and analysis of models of calcium dynamics based on IP3-sensitive calcium channel kinetics. *Biophys J* 70: 246–63.
37. Doedel EJ, Keller HB, Kernevez JP (1991) Numerical analysis and control of bifurcation problems: (I) Bifurcation in finite dimensions. *Int J Bifurc Chaos* 1: 493–520.
38. Doedel EJ, Keller HB, Kernevez JP (1991) Numerical analysis and control of bifurcation problems: (II) Bifurcation in infinite dimensions. *Int J Bifurc Chaos* 1: 745–772.
39. Bai Y, Edelmann M, Sanderson MJ (2009) The contribution of inositol 1,4,5-trisphosphate and ryanodine receptors to agonist-induced Ca²⁺ signaling of airway smooth muscle cells. *Am J Physiol Lung Cell Mol Physiol* 297: L347–61.
40. Berridge MJ (2009) *Cell Signalling Pathways*. In: *Cell Signalling Biology*, Portland Press, volume 3. pp. 2.1–2.118. Available: www.cellsignallingbiology.org.
41. Demaurex N, Frieden M (2003) Measurements of the free luminal ER Ca²⁺ concentration with targeted cameleon fluorescent proteins. *Cell Calcium* 34: 109–119.
42. Sneyd J, Tsaneva-Atanasova K, Yule DI, Thompson JL, Shuttleworth TJ (2004) Control of calcium oscillations by membrane fluxes. *PNAS* 101: 1392–6.
43. Shen WW, Frieden M, Demaurex N (2011) Local cytosolic Ca²⁺ elevations are required for stromal interaction molecule 1 (STIM1) de-oligomerization and termination of store-operated Ca²⁺ entry. *J Biol Chem* 286: 36448–59.
44. Malli R, Naghdi S, Romanin C, Graier WF (2008) Cytosolic Ca²⁺ prevents the subplasmalemmal clustering of STIM1: an intrinsic mechanism to avoid Ca²⁺ overload. *J Cell Sci* 121: 3133–9.
45. Shuttleworth TJ (1999) What drives calcium entry during [Ca²⁺]_i oscillations? – challenging the capacitative model. *Cell Calcium* 25: 237–46.
46. Bird GSJ, Putney JW (2005) Capacitative calcium entry supports calcium oscillations in human embryonic kidney cells. *J Physiol* 562: 697–706.
47. Trebak M (2011) PLC: Johnny-come-lately to ORAI and the ups and downs of calcium signalling. *J Physiol* 589: 5337–8.
48. Shuttleworth T (2012) STIM and Orai proteins and the non-capacitative ARC channels. *Front Biosci* 17: 847–860.
49. Jousset H, Frieden M, Demaurex N (2007) STIM1 knockdown reveals that store-operated Ca²⁺ channels located close to sarco/endoplasmic Ca²⁺ ATPases (SERCA) pumps silently refill the endoplasmic reticulum. *J Biol Chem* 282: 11456–64.
50. Mak DOD, McBride SMJ, Foskett JK (2003) Spontaneous channel activity of the inositol 1,4,5- trisphosphate (InsP3) receptor (InsP3R). Application of allosteric modeling to calcium and InsP3 regulation of InsP3R single-channel gating. *J Gen Physiol* 122: 583–603.
51. Gin E, Wagner LE, Yule DI, Sneyd J (2009) Inositol trisphosphate receptor and ion channel models based on single-channel data. *Chaos* 19: 037104.
52. Siekmann I, Wagner LE, Yule D, Crampin EJ, Sneyd J (2012) A Kinetic Model for type I and II IP3R accounting for mode changes. *Biophys J* 103: 658–68.
53. Manjarrés IM, Rodríguez-García A, Alonso MT, García-Sancho J (2010) The sarco/endoplasmic reticulum Ca²⁺ ATPase (SERCA) is the third element in capacitative calcium entry. *Cell Calcium* 47: 412–8.
54. Wang I, Politi AZ, Tania N, Bai Y, Sanderson MJ, et al. (2008) A mathematical model of airway and pulmonary arteriole smooth muscle. *Biophys J* 94: 2053–64.
55. Brook BS, Peel SE, Hall IP, Politi AZ, Sneyd J, et al. (2010) A biomechanical model of agonist-initiated contraction in the asthmatic airway. *Respir Physiol Neurobiol* 170: 44–58.
56. Politi AZ, Donovan GM, Tawhai MH, Sanderson MJ, Lauzon AM, et al. (2010) A multiscale, spatially distributed model of asthmatic airway hyper-responsiveness. *J Theor Biol* 266: 614–624.
57. Lauzon AM, Bates JHT, Donovan G, Tawhai M, Sneyd J, et al. (2012) A multiscale approach to airway hyperresponsiveness: from molecule to organ. *Front Physiol* 3: 191(1–25).
58. Brook BS, Jensen OE (2013) The role of contractile unit reorganization in force generation in airway smooth muscle. *Math Med Biol*. In press.
59. O'Donnell ME, Owen NE (1994) Regulation of ion pumps and carriers in vascular smooth muscle. *Physiol Rev* 74: 683–721.
60. Alberts B, Johnson A, Lewis J, Raff M, Roberts K, et al. (2008) *Molecular Biology of the cell*. New York: Garland, fifth edition. Available: <http://www.worldcat.org/isbn/0815332181>.
61. Lytton J, Westlin M, Burk SE, Shull GE, MacLennan DH (1992) Functional comparisons between isoforms of the sarcoplasmic or endoplasmic reticulum family of calcium pumps. *J Biol Chem* 267: 14483–9.